Available online at www.sciencedirect.com
ScienceDirect
International Journal of Heat and Mass Transfer 50 (2007) 216–225
International Journal of HEAT and MASS TRANSFER
www.elsevier.com/locate/ijhmt

# Matched asymptotic solution for the solute boundary layer in a converging axisymmetric stagnation point flow

Jānis Priede [a,b], Gunter Gerbeth [b,*]

[a] Institute of Physics, University of Latvia, LV-2169 Salaspils, Latvia
[b] Forschungszentrum Rossendorf, MHD Department, P.O. Box 510119, D-01314 Dresden, Germany

Received 30 November 2005; received in revised form 25 April 2006
Available online 24 August 2006

**Abstract**

A novel boundary-layer solution is obtained by the method of matched asymptotic expansions for the solute distribution at a solidification front represented by a disk of finite radius $R_0$ immersed in an axisymmetric converging stagnation point flow. The detailed analysis reveals a complex internal structure of the boundary layer consisting of eight subregions. The development of the boundary layer starts from the rim region where the concentration, according to the obtained similarity solution, varies with the radius $r$ along the solidification front as $\sim\ln^{1/3}(R_0/r)$. At intermediate radii, where the corresponding concentration is found to vary as $\sim\ln(R_0/r)$, the boundary layer has an inner diffusion sublayer adjacent to the solidification front, an inner core region, and an outer diffusion sublayer which separates the former from the outer uniformly mixed region. The inner core, where the solute transport is dominated by convection, is characterized by a logarithmically decreasing axial concentration distribution. The logarithmic increase of concentration along the radius is limited by the radial diffusion becoming effective in the vicinity of the symmetry axis at distances comparable to the characteristic thickness of the solute boundary layer.


*PACS:* 81.10.Aj; 81.10.Fq

*Keywords:* Mass transfer; Boundary layer; Analytical

## 1. Introduction

Solidification from the melt is usually accompanied by segregation of the dissolved substance which may be a component of an alloy or a dopant of a semi-conductor crystal. Despite the homogeneity of the original solution, the solidified material may have a non-uniform solute distribution. This non-uniformity stems from the difference of the equilibrium concentrations of the solute in the liquid and solid phases. Thus, if the equilibrium concentration of solute is lower in the solid than in the liquid phase, only a fraction of solute is incorporated from the solution into the solidifying material while the remaining part is repelled by the solidification front as it advances into the liquid phase [1]. This effect causes axial solute segregation that is usually concentrated in a thin, diffusion-controlled boundary layer adjacent to the solidification front. Axial segregation can strongly be affected by the melt convection. According to the classical work by Burton, Prim and Slichter (BPS) [2], a sufficiently strong convection towards the crystallization front reduces the thickness of the segregation boundary layer and so the solute concentration getting into the crystal. Such a concept of an effective solute boundary layer has been generally accepted to interpret the effect of melt flow on the solute distribution in various crystal growth applications [3–5].

The BPS approach, originally devised for a rotating-disk flow modeling an idealized Czochralski growth

* Corresponding author. Tel.: +49 351 2603484; fax: +49 351 2602007.
*E-mail address:* g.gerbeth@fz-rossendorf.de (G. Gerbeth).

0017-9310/$ - see front matter © 2006 Elsevier Ltd. All rights reserved.
doi:10.1016/j.ijheatmasstransfer.2006.06.016

**Nomenclature**

| | |
|---|---|
| $C$ | solute concentration |
| $C_0$ | uniform concentration of well-mixed solution |
| $C_1$ | scaled dimensionless variation of concentration |
| $\overline{C}_1^{\mathrm{c}}$ | inner core solution |
| $\widetilde{C}_1^{\mathrm{c}}$ | correction at the symmetry axis |
| $C_1^{\mathrm{o}}$ | outer core solution at symmetry axis |
| $D$ | diffusion coefficient |
| $d_0$ | characteristic thickness of the solute boundary layer |
| $F$ | similarity solutions at the rim and intermediate radii |
| $G^{\mathrm{c}}$, $G^{\mathrm{o}}$ | inner and outer core similarity solutions at the symmetry axis |
| $Pe_0$ | Péclet number based on the solidification velocity |
| $Sc$ | Schmidt number |
| $k$ | equilibrium partition coefficient |
| $R_0$ | dimensional radius of the disk |
| $R$ | dimensionless radius of the disk |
| $r$, $z$ | cylindrical coordinates |
| $v$ | melt velocity |
| $v_0$ | solidification velocity |
| $v_{\mathrm{s}}$ | velocity scale |

*Greek symbols*

| | |
|---|---|
| $\alpha$, $\beta$ | exponents of similarity solution |
| $\delta$ | matching constant |
| $\epsilon$, $\varepsilon$ | small parameters |
| $\eta$, $\tilde{\eta}$ | logarithmic axial coordinate |
| $\nu$ | kinematic viscosity |
| $\phi$ | dimensionless axial solute flux |
| $\tau$ | logarithmic radial coordinate |
| $\xi$ | similarity variable |
| $\zeta$, $\tilde{\zeta}$ | intermediate axial coordinates |

*Subscripts*

| | |
|---|---|
| $j$ | order of expansion |
| $r$ | radial component |
| $z$ | axial component |

*Superscripts*

| | |
|---|---|
| c | inner core |
| i | inner diffusion layer |
| m | intermediate layer |
| o | outer core and diffusion layer |

configuration, supposes the melt to be driven towards the solidification front by a radially diverging flow. However, in many cases the melt is driven away from the solidification front in its central part by a radially converging flow. Examples are the flow rotating over a disk at rest [6], like in a flow driven by a rotating [7] or a traveling [8] magnetic field, as well as in the natural convection above a concave solidification front in the vertical Bridgman growth process [9]. Recently, we showed that the BPS approach is not applicable to converging flows directed away from the solidification front because the integral defining the effective boundary layer thickness, which is the basic concept of the BPS theory, becomes unbounded for such flows [10]. Our main conclusion was that a sufficiently strong melt flow away from the solidification front is not compatible with a radially uniform solute distribution. We considered a solidification front as a disk of finite radius embedded in a melt with a strong converging flow and found analytically a logarithmic solute segregation along the solidification front. The solution, which was obtained by a Laplace transform, was limited to the solidification front excluding the symmetry axis. Thus, we predicted the formation of a logarithmic concentration peak at the symmetry axis but could not calculate its amplitude.

In the present work, we extend our previous study and obtain a novel boundary-layer solution for the solute distribution directly at and ahead of the solidification front presented by a disk of finite size in a strong converging stagnation-point flow as in [10]. The solution, obtained by the method of matched asymptotic expansions [11], reveals a boundary layer with a complex structure consisting of seven sublayers and a corner region at the symmetry axis. For most of the subregions, the particular asymptotic solutions are obtained analytically except the outer diffusion layer, which separates the inner and outer core regions, and the corner region at the symmetry axis, where the corresponding asymptotic solutions can be found only numerically. Each particular asymptotic solution is validated by comparing with the numerical solution of the original problem.

The paper is organized as follows. In Section 2, the problem for a disk of finite radius in a strong converging axisymmetric neutral point flow is formulated. A similarity solution at the rim, and matched asymptotic expansions at intermediate radii and at the symmetry axis are obtained in Sections 3–5, respectively. The obtained solution is discussed in Section 6 and conclusions are presented in Section 7.

## 2. Formulation of the problem

Consider a solidification front as a disk of finite radius $R_0$ advancing upwards with velocity $v_0$ into an unbounded volume of melt which is a dilute solution characterized by the solute concentration $C$, as shown in Fig. 1. Sufficiently far away from the solidification front, the melt is assumed to be well-mixed with uniform concentration $C_0$. At the solidification front, supposed to be at the thermodynamic

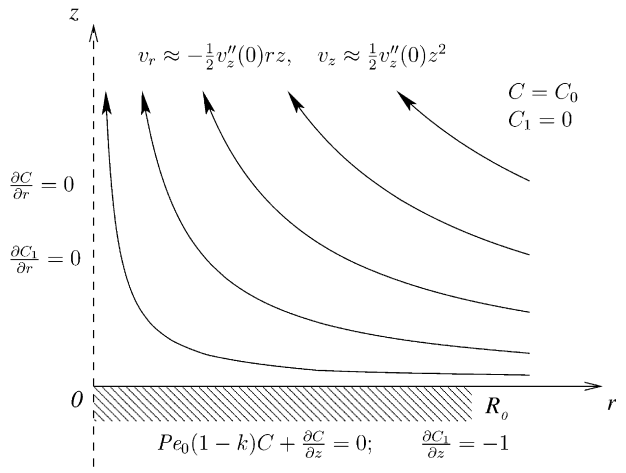


Fig. 1. Sketch of the solidification front presented by a disk of radius $R_0$ in a converging stagnation point flow with radial and axial velocity components $v_r$ and $v_z$ including the boundary conditions for the concentration $C$ and the dimensionless deviation $C_1$ from the uniform concentration $C_0$ of a well-mixed melt core.

equilibrium, the ratio of solute concentrations in the solid and liquid phases is given by the equilibrium partition coefficient $k$. In the melt, solute is transported by both diffusion with a coefficient $D$ and convection with a velocity field $\vec{v}$. For simplicity, the latter is assumed here to be similar to the velocity distribution in a liquid rotating above a fixed flat wall [6]. Thus, the axial velocity is assumed to depend only on the vertical distance from the solidification front, similarly to the rotating disk flow in the classical BPS formulation [2], but the direction of the flow is opposite in our case. In addition, we consider as usual the solute boundary layer to be much thinner than that of momentum which corresponds to large Schmidt numbers $Sc = \nu/D$, where $\nu$ is the kinematic viscosity of the melt. Then, the radial and axial velocity components satisfying incompressibility, impermeability and no-slip constraints can be approximated by the first terms of the corresponding power series expansions in $z$

$$v_r \approx -\frac{1}{2}v_z''(0)rz, \quad v_z \approx \frac{1}{2}v_z''(0)z^2. \tag{1}$$

These expressions represent, on one hand, the simplest description of a boundary layer flow as sketched in Fig. 1. Since, on the other hand, the solute boundary layer investigated here is due to $Sc \gg 1$ much smaller than the velocity boundary layer, Eq. (1) represents to a leading order also the general velocity structure of the considered converging flow. Hence, the use of the simple expressions (1) is expected to illustrate the effect of radial segregation in more general converging flows.

Henceforth, we use the thickness of the solute boundary layer based on the axial melt velocity as length scale

$$d_0 = (2D/v_z''(0))^{1/3} \tag{2}$$

and $C_0$ as the characteristic concentration scale to nondimensionalize all variables by keeping the original notation. In addition, we assume the stirring of the melt to be so strong that the advancement of the solidification front with the growth velocity $v_0$ is small compared the characteristic melt velocity in the solute boundary layer. The last assumption implies that the local Péclet number based on the growth rate is small: $Pe_0 = v_0 d_0/D \ll 1$. Then the problem is defined by a single dimensionless parameter, the dimensionless radius $R = R_0/d_0 = R_0(2D/v_z''(0))^{-1/3}$, which may be regarded as Péclet number based on the external length scale $R_0$ and the internal velocity scale $v_s = v_z''(0)d_0^2/2$. The governing dimensionless equation is

$$z\left(z\frac{\partial C}{\partial z} - r\frac{\partial C}{\partial r}\right) = \frac{1}{r}\frac{\partial}{\partial r}\left(r\frac{\partial C}{\partial r}\right) + \frac{\partial^2 C}{\partial z^2}, \tag{3}$$

where the radial diffusion term will be neglected as usual for the boundary layer solution along the solidification front obtained in the following.

By taking into account that sufficiently far away from the solidification front the concentration tends to a constant value of the well-mixed melt that in dimensionless form reads as $C|_{z\to\infty} = 1$, the boundary condition at the solidification front

$$Pe_0(1-k)C + \left.\frac{\partial C}{\partial z}\right|_{z=0} = 0$$

with $Pe_0 \ll 1$ suggests to search for the concentration as

$$C \approx 1 + Pe_0(1-k)C_1, \tag{4}$$

where $C_1$ is the dimensionless deviation of the concentration with a characteristic magnitude $Pe_0(1-k) \ll 1$ from its uniform core value. Consequently, the boundary conditions for $C_1$ take the form

$$\left.\frac{\partial C_1}{\partial z}\right|_{z=0} = -1 \tag{5}$$

and $C_1|_{z\to\infty} = 0$, while $C$ is replaced by $C_1$ in Eq. (3) which, in comparison to the original BPS equation, has an extra term related to the radial advection whereas the term of axial advection due to the solidification speed is neglected [2]. Searching for similarity solutions along the solidification front in the form $C_1(r,z) = r^\alpha F(zr^\beta)$ leads to radially uniform solutions only with $\alpha = \beta = 0$ which were shown in our previous study [10] to become unbounded for this type of converging flow. However, similarity solutions can be obtained for this problem after elimination of $r$ from Eq. (3) that is accomplished by the substitution $\tau = -\ln(r)$ leading to

$$z\left(z\frac{\partial C}{\partial z} + \frac{\partial C}{\partial \tau}\right) = \frac{\partial^2 C}{\partial z^2}. \tag{6}$$

Since this equation does not explicitly contain $\tau$, $C(\tau, z)$ being a solution implies that $C(\tau - \tau_0, z)$ is also a solution. Consequently, we can replace $\tau$ by $\tau - \tau_0$, where $\tau_0 = -\ln(R)$ and thus $\tau = \ln(R/r)$. Note that $\tau = 0$ corresponds to the rim of the disk while $\tau \to \infty$ to the symmetry axis. Now, a similarity solution can be sought as

$$C(\tau,z)=\tau^{\alpha}F(\xi), \tag{7}$$

where $\xi=z\tau^{\beta}$, that substituted into Eq. (6) results in

$$\xi(\tau\xi F'+\alpha F+\beta\xi F')=\tau^{1+3\beta}F''. \tag{8}$$

## 3. Similarity solution at the rim

Neglecting the term proportional to $\tau$ that is expected to be small at the rim we find $\beta=-\frac{1}{3}$ while Eq. (8) takes the form

$$F_0''+\frac{\xi}{3}(\xi F_0'-F_0)=0,$$

but the boundary condition (5) yields $\alpha=-\beta=\frac{1}{3}$ and

$$F_0'(0)=-1. \tag{9}$$

The solution of the above equation satisfying the boundary condition at infinity is

$$F_0(\xi)=c_0\exp\left(-\frac{\xi^3}{9}\right)U\left(1,\frac{2}{3},\frac{\xi^3}{9}\right), \tag{10}$$

where $U(a,b,x)$ is the confluent hypergeometric function [12]. From boundary condition (9) we find $c_0=3^{-1/3}/\Gamma(2/3)$. Consequently, the radial solute segregation along the solidification front at the rim is given by $C_1(r,0)=\ln^{1/3}(R/r)F_0(0)$, where $F_0(0)=3^{2/3}/\Gamma(2/3)\approx 1.5361$. Note that the obtained solution is valid only for $\tau\ll 1$ because the neglected term becomes significant at $\tau\sim 1$. This neglected term can be taken into account by searching for solutions in the more general form

$$C_1(\tau,z)=\tau^{\alpha}F(\xi;\tau)=\tau^{\alpha}\sum_{j=0}\tau^{j}F_j(\xi). \tag{11}$$

Substitution of this solution into Eq. (6) leads to the recursive system of equations:

$$F_j''+\frac{\xi}{3}(\xi F_j'-(1+3j)F_j)=\xi^2F_{j-1}',$$
$$F_j'(0)=\begin{cases}-1, & j=0\\ 0, & j>0\end{cases}. \tag{12}$$

The solution for $j=0$ is already found above. For $j=1$ the solution is

$$F_1(\xi)=c_1\exp\left(-\frac{\xi^3}{9}\right)U\left(2,\frac{2}{3},\frac{\xi^3}{9}\right)+\left(1+\frac{\xi^3}{6}\right)F_0(\xi). \tag{13}$$

From the boundary condition in (12) we find $c_1=-c_0$ and, thus, the first correction to the radial solute segregation at the rim to be $F_1(0)=\frac{1}{4}F_0(0)$. Although no further analytic solutions for $j>1$ can be found in this way, the exact expressions for all coefficients $F_j(0)$, which define the concentration distribution along the solidification front, can be derived analytically [10] by applying a Laplace transform directly to Eq. (6) with neglected radial diffusion term. The similarity solutions (10) and (13) are plotted in Fig. 2 while the corresponding concentration distributions

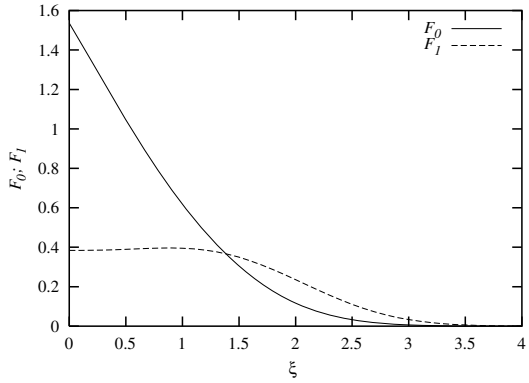


Fig. 2. First two terms of the similarity solution defined by (10) and (13) versus the similarity variable $\xi=z/\tau^{1/3}$.

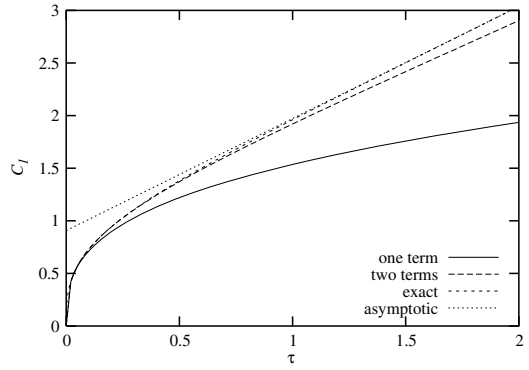


Fig. 3. Comparison of different approximations for the concentration distribution along the solidification front versus $\tau=\ln(R/r)$: one and two terms of the similarity solution at the rim (11), exact solution obtained in [10], and intermediate asymptotic solution (15).

along the solidification front are shown in Fig. 3 together with the intermediate asymptotic solution obtained in the following section and the exact power-series solution obtained in [10].

## 4. Intermediate matched asymptotic expansions

### 4.1. Inner diffusion and intermediate layers

At large distances from the rim, the first term in Eq. (8) proportional to $\tau$ becomes dominant. To balance this term with the r.h.s. of the equation we have to choose $\beta=0$ that transforms Eq. (8) into

$$F''-z(zF'+\epsilon F)=0, \tag{14}$$

where $\epsilon=\alpha/\tau$ may be regarded as a small parameter for $\tau\gg 1$; and $\alpha$ is an unknown constant appearing also in the boundary condition $\tau^{\alpha}F'(0)=-1$. Note that by ignoring the small term we recover again the classical BPS problem having no bounded solution that implies the solution to diverge as $\epsilon\to 0$. The key to the solution is the appearance of the small term in Eq. (14) as a factor at the coordinate. Thus, however small is $\epsilon$, the corresponding product

becomes $\sim 1$ at $z \sim 1/\epsilon$ which is an essential length scale of the problem missed by the BPS approach.

The problem above can be solved by the method of matched asymptotic expansions [11]. The solution, which because of its length and complexity is presented in Appendix A, yields the solute distribution along the solidification front sufficiently far away from the rim

$$C_1(r,0) = c_0\left(\ln\left(\frac{R}{r}\right) + c_1\right) + \mathrm{O}\left(\ln^{-1}\left(\frac{R}{r}\right)\right), \tag{15}$$

where the constants $c_0$ and $c_1$ are given by (31) and (35). This solution plotted versus $\tau = \ln(R/r)$ in Fig. 3 is seen to match the exact power series solution obtained in [10] surprisingly well already at $\tau > 1$.

Alternatively, the above asymptotic solution can be obtained by first solving Eq. (14) exactly as

$$F(z;\epsilon) = \frac{3^{1/3}\Gamma(1+\epsilon/3)}{\Gamma(2/3)}\, U\left(\frac{\epsilon}{3}, \frac{2}{3}, \frac{z^3}{3}\right) \tag{16}$$

and then taking the first two terms of the power-series expansion in $\epsilon$. Note that (16) has the same asymptotics as the intermediate solution considered above. Thus, (16) presents a composite solution valid up to the first order in $\epsilon$ in both the inner diffusion layer and intermediate regions. However, it will be shown later that the first two terms of the asymptotic solution present an accurate solution of the original problem for a larger range of $z$ than (16) whose accuracy is limited to a certain neighborhood of the solidification front. This is because Eq. (14), as shown previously, is accurate only up to the first order in $\epsilon$.

### 4.2. Inner core region

The comparison with a numerical solution of Eq. (6), obtained by a Chebyshev collocation method with an algebraic mapping to a semi-infinite domain for $z$ and a Crank–Nicolson scheme for $\tau$ [13], shows that (16) is accurate only in the vicinity of the solidification front (see Fig. 4a). The discrepancy between the asymptotic and the numerical solutions at larger distances from the solidification front is obviously due to the higher-order small term neglected in Eq. (14). With this term taken into account Eq. (14) reads as

$$z\left(z\frac{\partial F}{\partial z} + \epsilon F - \epsilon^2\frac{\partial F}{\partial \epsilon}\right) = \frac{\partial^2 F}{\partial z^2}. \tag{17}$$

Note that for the intermediate solution $F \sim z^{-\epsilon}$ we have $\frac{\partial F}{\partial \epsilon} \sim -\ln(z)F$. Thus, the neglected term becomes comparable to the retained one at $\epsilon\ln(z) \sim 1$. This fact as well as $z^{-\epsilon} \approx 1 - \epsilon\ln(z)$ for $\epsilon\ln(z) \ll 1$ suggests that the solution at $z \gg 1$ and $\epsilon\ln(z) \ll 1$ can be sought in terms of a new coordinate $\eta = \epsilon\ln(\delta z)$, where $\delta$ is a constant to be determined by matching with the intermediate solution. Henceforth we refer to this region as the inner core because here the concentration distribution is dominated by convection similarly to the outer core region. At the leading order in $\epsilon$, Eq. (17) takes the form

$$-(\eta - 1)\frac{\mathrm{d}F_0^{\mathrm{c}}}{\mathrm{d}\eta} + F_0^{\mathrm{c}} = 0.$$

Note that exponentially small terms have been neglected in the above equation whose solution is

$$F_0^{\mathrm{c}}(\eta) = c_0^{\mathrm{c}}(1-\eta), \tag{18}$$

where $c_0^{\mathrm{c}}$ is a constant to be determined from matching with the intermediate solution:

$$\begin{aligned} F^{\mathrm{m}}(z) &= c_0(1-\epsilon\gamma/3)\left(3^{-1/3}z\right)^{-\epsilon} + \mathrm{O}(\epsilon^2) \\ &= c_0(1-\epsilon(\gamma-\ln 3)/3 - \epsilon\ln(z)) + \mathrm{O}(\epsilon^2) \end{aligned}$$

yielding

$$\delta = \left(\frac{\mathrm{e}^{\gamma}}{3}\right)^{1/3} \tag{19}$$

and $c_0^{\mathrm{c}} = c_0$. Solution (18) is seen in Fig. 4b to be in good agreement with the numerical one plotted against the rescaled coordinate $\tau(\eta - 1) = \ln(\delta z e^{-\tau})$. Note that the inner core solution matches the intermediate layer solution in the same range as the latter matches the inner diffusion layer because in both cases we use the condition $\epsilon\ln(z) \ll 1$. In this way, the inner core solution matches directly with the inner diffusion layer solution and, thus, the

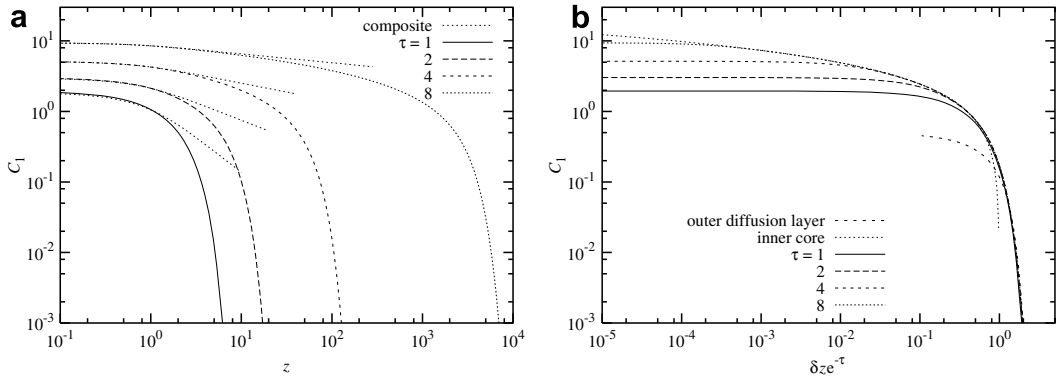


Fig. 4. Numerically obtained axial concentration profiles at several radial positions defined by $\tau = \ln(R/r)$ together with the composite solution (16) (a) and the inner core (18) and outer diffusion layer (23) solutions (b) versus the original (a) and rescaled (b) coordinates.

intermediate solution is no longer necessary. Moreover, according to Eq. (33) for $z \gg 1$ the asymptotics of the leading and first-order inner diffusion layer coincide with the inner core solution. Thus the first two terms of the inner diffusion layer solution present a composite solution valid also in the inner core region.

### 4.3. Outer diffusion layer

The agreement with the numerical solution holds only up to $\eta \approx 1$ because (18) becomes negative for $\eta > 1$. This suggests that there has to be an additional transition region between the inner and outer core regions where the adjustment of concentration to its uniform value in the outer core is ensured by diffusion. For the diffusion term to become significant, the outer diffusion layer has to be thin enough. To describe this layer we introduce a new stretched coordinate $\varepsilon\tilde{\eta} = \eta - 1 = \epsilon \ln(\delta z) - 1$, where $\varepsilon$ is a small parameter regarded to be a function of $\epsilon$. Matching with the inner core solution $F_0^{\mathrm{c}}(\eta) = c_0(1-\eta) = -c_0\varepsilon\tilde{\eta}$ suggests that the solution in the outer diffusion layer can be sought as $F(z,\tau) = \varepsilon F^{\mathrm{o}}(\tilde{\eta})$. Substitution of this ansatz into Eq. (17) results in

$$\left(1 - \frac{\epsilon}{\varepsilon}\frac{\mathrm{d}\varepsilon}{\mathrm{d}\epsilon}\right)\left(-\tilde{\eta}\frac{\mathrm{d}F^{\mathrm{o}}}{\mathrm{d}\tilde{\eta}} + F^{\mathrm{o}}\right) = \delta^3 \mathrm{e}^{-3(1+\varepsilon\tilde{\eta})/\epsilon}\frac{\epsilon}{\varepsilon^2}\left(\frac{\mathrm{d}^2F^{\mathrm{o}}}{\mathrm{d}\tilde{\eta}^2} - \frac{\varepsilon}{\epsilon}\frac{\mathrm{d}F^{\mathrm{o}}}{\mathrm{d}\tilde{\eta}}\right), \tag{20}$$

where the relation $\frac{\mathrm{d}\tilde{\eta}}{\mathrm{d}\epsilon} = -\frac{\tilde{\eta}}{\varepsilon}\frac{\mathrm{d}\varepsilon}{\mathrm{d}\epsilon}$ has been taken into account. To balance the diffusion term on the r.h.s. of the above equation with the advection term, the thickness of the transition layer has to satisfy

$$1 - \frac{\epsilon}{\varepsilon}\frac{\mathrm{d}\varepsilon}{\mathrm{d}\epsilon} = \delta^3 \mathrm{e}^{-3/\epsilon}\frac{\epsilon}{\varepsilon^2}. \tag{21}$$

Searching for an asymptotic solution of the above equation as $\varepsilon(\epsilon) \sim \varepsilon_0(\epsilon) + \varepsilon_1(\epsilon) + \cdots$ we obtain $\varepsilon_0 = \lambda\epsilon$ and $\varepsilon_1 = -\frac{1}{3}\epsilon \mathrm{e}^{-3/\epsilon}\delta^3/\lambda$, where $\lambda$ is an unknown constant. Since $\varepsilon_1$ presents an exponentially small correction to $\varepsilon_0$, we have $\varepsilon \approx \lambda\epsilon$ for $\epsilon \ll 1$. Note that from the physical point of view the outer diffusion layer is formed by two competing effects due to convection. On one hand, the concentration profile is advected by the tangential velocity along the streamline and smoothed out by diffusion. On the other hand, the normal velocity component developing across the layer tries to reduce its thickness. These counteracting effects, described by Eq. (21), result in an equilibrium diffusion layer thickness $\varepsilon = \mathrm{O}(\epsilon)$ at which Eq. (20) in leading order takes the form

$$-\tilde{\eta}\frac{\mathrm{d}F_0^{\mathrm{o}}}{\mathrm{d}\tilde{\eta}} + F_0^{\mathrm{o}} = \mathrm{e}^{-3\lambda\tilde{\eta}}\left(\frac{\mathrm{d}^2F_0^{\mathrm{o}}}{\mathrm{d}\tilde{\eta}^2} - \lambda\frac{\mathrm{d}F_0^{\mathrm{o}}}{\mathrm{d}\tilde{\eta}}\right). \tag{22}$$

Eq. (22) contains an unknown constant $\lambda$ which may be related to the initial condition for $\varepsilon$ at the edge of the disk at $\tau = 0$ corresponding to $\epsilon \to \infty$. This can be done by considering the exact solution of Eq. (21) $\varepsilon(\epsilon) = \epsilon\sqrt{\lambda^2 - \frac{3}{2}\delta^3\mathrm{e}^{-3/\epsilon}}$. By requiring $\varepsilon$ to vanish at the edge of the disk $\tau = 1/\epsilon = 0$, where the boundary layer starts to form, we obtain $\lambda = \sqrt{2\delta^3/3} = \sqrt{2\mathrm{e}^{\gamma}}/3 \approx 0.62912$. Although there is no rigorous argument for such a choice of $\lambda$, the corresponding solution of Eq. (22) turns out to be very close to the numerical solution (see Fig. 4b). Eq. (22) can be solved only numerically. For this purpose we first redefine the coordinate as $\tilde{z} = \mathrm{e}^{\lambda\tilde{\eta}} = \delta\mathrm{e}^{-\tau}z$ that transforms Eq. (22) into

$$\lambda^2\frac{\mathrm{d}^2F_0^{\mathrm{o}}}{\mathrm{d}\tilde{z}^2} + \tilde{z}\left(\tilde{z}\ln\tilde{z}\frac{\mathrm{d}F_0^{\mathrm{o}}}{\mathrm{d}\tilde{z}} - F_0^{\mathrm{o}}\right) = 0. \tag{23}$$

Now, the above equation can easily be solved numerically by a Chebyshev collocation method in the semi-infinite interval for $\tilde{z}$ by specifying $F_0^{\mathrm{o}}|_{\tilde{z}=0} = c_0^{\mathrm{o}}$ and $F_0^{\mathrm{o}}|_{\tilde{z}\to\infty} \to 0$. In this case, $\lambda$ determines the extension of the solution beyond $\tilde{z} \approx 1$ while $c_0^{\mathrm{o}}$ should in principle be determined by matching with the outer solution at $\tilde{z} \leqslant 1$. However, there is no defined matching procedure because $c_0^{\mathrm{o}}$ is specified by the boundary condition at $\tilde{z} = 0$ whereas Eq. (23) is valid only in a certain neighborhood of $\tilde{z} = 1$. Thus, on the one hand, the numerical solution is determined up to an arbitrary factor $c_0^{\mathrm{o}}$, but on the other hand the particular choice of $c_0^{\mathrm{o}}$, provided that $c_0^{\mathrm{o}} \sim 1$, has a minor effect on the extension of the solution at $\tilde{z} > 1$ which is determined essentially by $\lambda$. Thus the numerical solution allows us to asses $\lambda$ without an exact matching with the outer solution.

## 5. Boundary layer at the symmetry axis

### 5.1. Inner axial layer

According to the solution obtained in the previous section (Eq. (15)), the solute concentration along the solidification front increases towards the symmetry axis as $\sim\ln(r)$. Such a solution becomes singular at $r = 0$ and, thus, it cannot predict the magnitude of the concentration perturbation at the symmetry axis. This singularity is due to the neglected radial diffusion term in Eq. (3) which obviously becomes significant at $r \sim 1$. In order to obtain a bounded solution at the symmetry axis we take into account the radial diffusion term but, at first, neglect the axial diffusion term by considering $z \gg 1$. Then the equation governing the concentration perturbation $C_1$ defined by (4) takes the form

$$z\left(z\frac{\partial C_1}{\partial z} - r\frac{\partial C_1}{\partial r}\right) = \frac{1}{r}\frac{\partial}{\partial r}\left(r\frac{\partial C_1}{\partial r}\right), \tag{24}$$

while the boundary condition at the axis reads as $\frac{\partial C_1}{\partial r}\big|_{r=0} = 0$. Note that the axial diffusion term was neglected also for the inner core region considered in Section 4.2. Thus, the solution of Eq. (24) is expected to match at $r \to \infty$ with the radial inner core solution (18) which in the original variables reads as $\overline{C}_1^{\mathrm{c}}(r,z) = \tau F_0^{\mathrm{c}}(\eta) = -c_0\ln(\delta r z/R)$, where $\delta$ is defined by (19). It is easy to see that $\overline{C}_1^{\mathrm{c}}(r,z)$ satisfies Eq. (24) but not the boundary condition at the axis where it has a singularity. This suggests a

search for the solution at the symmetry axis as $C_1^c(r,z) = \overline{C}_1^c(r,z) + \widetilde{C}_1^c(r,z)$, where $\widetilde{C}_1^c$ is a correction satisfying Eq. (24) and the boundary condition

$$\frac{\partial \widetilde{C}_1^c}{\partial r} \to -\frac{\partial \overline{C}_1^c}{\partial r} = \frac{c_0}{r} \quad \text{as } r \to 0. \tag{25}$$

We again look for a similarity solution in the form $\widetilde{C}_1^c(r,z) = z^\alpha G^c(\xi)$, where $\xi = rz^\beta$. By substituting this solution into Eq. (24) and into the boundary condition (25) we find, respectively, $\beta = \frac{1}{2}$ and $\alpha = 0$. Then the corresponding equation takes the form

$$\frac{1}{\xi}\frac{\mathrm{d}}{\mathrm{d}\xi}\left(\xi\frac{\mathrm{d}G^c}{\mathrm{d}\xi}\right) + \frac{\xi}{2}\frac{\mathrm{d}G^c}{\mathrm{d}\xi} = 0.$$

The solution of this equation satisfying (25) and vanishing at $r \gg 1$ is $G^c(\xi) = -\frac{1}{2}c_0 E_1(\xi^2/4)$, where $E_1(x)$ is the exponential integral [12]. This solution shows that there is a boundary layer around the symmetry axis with a characteristic radial size that decreases as $\sim z^{-1/2}$ with distance $z$ from the solidification front. Radial diffusion in this axial boundary layer smoothes out the concentration peak caused by the converging flow and so limits the magnitude of the concentration perturbation at the symmetry axis. With this correction the concentration distribution along the symmetry axis is

$$C_1^c(0,z) = \frac{c_0}{2}\ln\left(\frac{3\delta R^2}{4z}\right). \tag{26}$$

Note that similarly to the radial inner core solution the above solution along the axis becomes invalid at both small and large distances from the solidification front. First, the solution diverges at $z \to 0$ because of the neglected axial diffusion term expected to become important at the solidification front. Second, the solution also diverges at large distances, becoming negative for $z > 3/4\delta R^2$.

### 5.2. Outer axial layer

At sufficiently large axial distances, the boundary layer forming along the symmetry axis is expected to extend from the inner core region into the outer one. Similarly to the inner core, the concentration distribution in this outer axial region is supposed to be governed by Eq. (24). The difference to the inner core region is that now the axial boundary layer is surrounded by the uniformly mixed outer core implying $C_1|_{r\to\infty} \to 0$. The solution in this outer axial layer is sought similarly to the inner one as $C_1^o(r,z) = z^\alpha G^o(\xi)$, where $\xi = rz^\beta$. This leads to $\beta = \frac{1}{2}$ and the equation

$$\frac{1}{\xi}\frac{\mathrm{d}}{\mathrm{d}\xi}\left(\xi\frac{\mathrm{d}G^o}{\mathrm{d}\xi}\right) + \frac{\xi}{2}\frac{\mathrm{d}G^o}{\mathrm{d}\xi} - \alpha G^o = 0, \tag{27}$$

while the boundary condition at the symmetry axis takes the form $\left.\frac{\mathrm{d}G^o}{\mathrm{d}\xi}\right|_{\xi=0} = 0$. The remaining unknown constant $\alpha$ is determined in this case from the solute conservation as follows. The axial solute flux through a surface parallel to the solidification front at sufficiently large axial distance is

$$\phi = 2\pi\int_0^\infty rz^2 C_1^o(r,z)\,\mathrm{d}r = 2\pi z^{1+\alpha}\int_0^\infty G^c(\xi)\xi\,\mathrm{d}\xi.$$

Solute conservation requires this flux to be a constant, i.e., invariant with respect to $z$, that results in $\alpha = -1$. Then the solution of Eq. (27) is

$$G^o(\xi) = G_0^o \exp\left(-\frac{\xi^2}{4}\right),$$

where $G_0^o$ is a constant related to the axial solute flux $\phi = 4\pi G_0^o$ that in turn is equal to the solute flux into the melt from the solidification front which in the approximation of strong mixing is

$$\phi = -2\pi\int_0^R \left.\frac{\partial C_1}{\partial z}\right|_{z=0} r\,\mathrm{d}r = \pi R^2.$$

In the original variables, we obtain $C_1^o(r,z) = R^2/(4z)\exp(-r^2 z/4)$. Matching with the inner core region, where $C_1^c(0,z) = \mathrm{O}(1)$ in terms of $R \gg 1$, implies that the transition from the inner to the outer solution takes place at $z_c \sim R^2$ that defines the characteristic axial extension of the inner core region. Note that this is also the point of intersection of the axial boundary layer $r \sim z^{-1/2}$ and the outer edge of the inner core region $z \sim R/r$. Both the inner and outer axial asymptotic solutions are confirmed by the full numerical solution of the finite disk problem as shown in Fig. 5.

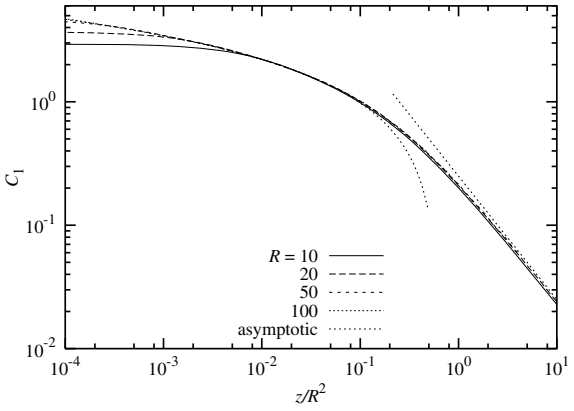


Fig. 5. Dimensionless concentration perturbations $C_1$ along the symmetry axis resulting from the full numerical solution for disks of various dimensionless radii $R$ together with inner and outer axial asymptotic solutions against the rescaled axial coordinate $z/R^2$.

### 5.3. Corner region

The axial inner core solution (26) diverges close to the solidification front since the axial diffusion term neglected in Eq. (24) becomes significant in the inner diffusion layer at $z \sim 1$. This term taken into account leads back to the original governing equation (3). Now we can take the advantage of the known asymptotic inner core solutions to solve

for the concentration distribution only in the enclosed corner region at the symmetry axis rather than in the whole domain above the disk. Thus, the leading and first order radial asymptotic solutions obtained in Section 4.1 yield

$$C_1(r,z) \to \tau\left(F_0^{\mathrm{i}}(z) + \epsilon F_1^{\mathrm{i}}(z)\right) = c_0 \ln\left(\frac{R}{r}\right) + F_1^{\mathrm{i}}(z), \quad r \to \infty$$

that in turn implies

$$r\frac{\partial C_1}{\partial r}\bigg|_{r\to\infty} = -c_0.$$

Note that the latter boundary condition is preferred for the following numerical solution because it does not involve $F_1^{\mathrm{i}}(z)$ defined by the rather complicated expression (32). Similarly, the axial inner core solution from Section 5.1 yields

$$C_1(r,z) \to c_0\left(\ln\left(\frac{R}{\delta r z}\right) - \frac{1}{2}E_1\left(\frac{r^2 z}{4}\right)\right), \quad z \to \infty$$

that also implies

$$z\frac{\partial C_1}{\partial z}\bigg|_{z\to\infty} = -c_0.$$

In addition, we have two original boundary conditions, one at the solidification front $\frac{\partial C_1}{\partial z}\big|_{z=0} = -1$ and one at the symmetry axis $\frac{\partial C_1}{\partial r}\big|_{r=0} = 0$. Note that the replacement of the original Dirichlet boundary conditions by simpler Neumann-type boundary conditions at the outer edge of the inner core region results in the concentration defined up to an additive constant. In order to have a correctly posed problem for the numerical solution we impose an additional condition by fixing the concentration in the corner point: $C_1(0,0) = 0$. In this case, the problem is too complicated to be solved analytically and, thus, we resort to a numerical solution using a Chebyshev collocation method [13] with an additional algebraic coordinate mapping. The calculated concentration distributions along both the solidification front and the symmetry axis are plotted in Fig. 6 together with the corresponding asymptotic solutions

$$C_1(r,0) = c_r - c_0 \ln(r),$$
$$C_1(0,z) = c_z - \frac{c_0}{2}\ln(z),$$

where $c_r \approx 0.3772$ and $c_z \approx -0.7751$ are determined from the best fit of the numerical solution. Note that according to the asymptotic solutions (15) and (26) $c_r - c_z = c_0(c_1 - \frac{1}{2}\ln(3\delta/4)) = 1.1528$, where $c_0$, $c_1$ and $\delta$ are defined by Eqs. (31), (35) and (19), respectively, that agrees well with the numerical solution. Further, matching with (15) yields $C_1(0,0) = c_0(\ln(R) + c_1) - c_r$.

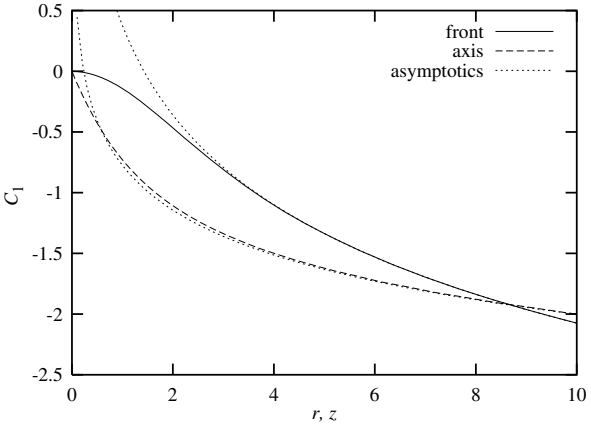


Fig. 6. Numerically calculated concentration distributions in the corner region along both the solidification front and the symmetry axis together with the corresponding asymptotics.

## 6. Discussion

The obtained solution reveals a complex internal structure of the solute boundary layer consisting of several characteristic regions and sublayers which are shown schematically in Fig. 7. The boundary layer develops from the rim region of the disk having a width of the same order of magnitude as the characteristic solute boundary layer thickness $d_0$ defined by Eq. (2) which represents an internal length for the boundary layer under consideration. The rim region is succeeded towards the axis by an inner diffusion layer (c) located adjacent to the solidification front and having the characteristic thickness $\sim d_0$. The inner diffusion layer is connected to the inner core region (d), where the solute transport is dominated by convection similarly to the bulk of the melt referred to as the outer core region (a). The inner core region is bounded from the side of the outer one by the streamline defined as $r = \delta d_0 R_0/z$, where $\delta$ is the dimensionless constant given by Eq. (19). The inner core region has a characteristic axial solute segregation that decreases logarithmically with distance from the

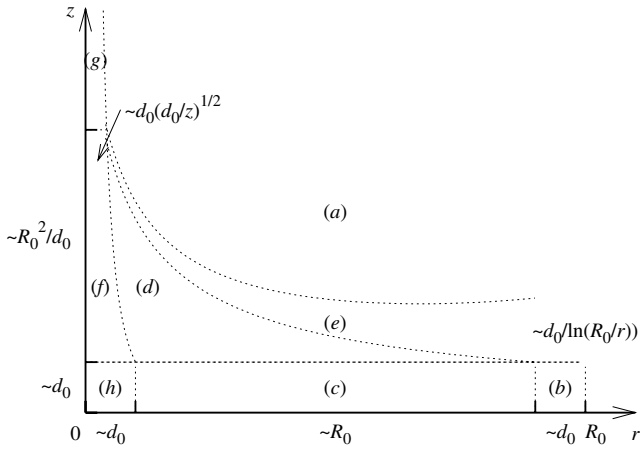


Fig. 7. Principal structure of the solute boundary layer in a converging flow over a solidification front of finite radius $R_0$ showing various subregions and their characteristic sizes: (a) outer core, (b) rim, (c) inner diffusion layer, (d) inner core; (e) outer diffusion layer; (f) inner axial layer; (g) outer axial layer; (h) corner region. The internal length scale given by the characteristic solute boundary layer thickness $d_0$ is defined by Eq. (2).

solidification front. The outer edge of the inner core is defined by the position where the logarithmically decreasing concentration perturbation becomes formally negative. At this point, the outer diffusion layer (e) forms by separating the inner and outer core regions. The characteristic thickness of this sublayer decreases towards the symmetry axis as $\sim d_0(1/\ln(R_0/r))$. Diffusion becomes significant in this thin transition layer and ensures that the concentration of the inner core smoothly matches with the outer one without becoming negative as it would follow from the inner core solution alone. The boundary layer changes in the vicinity of the symmetry axis where the radial diffusion becomes significant by smoothing out the logarithmically growing solute concentration. Three characteristic subregions can be distinguished along the symmetry axis. First, there is an axial layer consisting of inner (f) and outer (g) parts which have a characteristic radial size decreasing as $\sim d_0(d_0/z)^{1/2}$ with distance $z$ from the solidification front. The inner part of this layer with axial extension $\sim R_0^2/d_0$ bounds radially with the inner core region and has a logarithmic axial solute distribution similar to that in the inner core region. The outer part of the axial layer extends from the inner core region into the outer one where the axial segregation starts to decrease along the symmetry axis inversely with the axial distance: $\sim R_0/z$. At the solidification front, the axial layer is bounded by the corner region (h), which is the third axial subregion with characteristic radial and axial sizes $\sim d_0$. In this region, both the radial and the axial diffusion becomes important. Thus, on one hand, the non-uniformity of the solute concentration increasing logarithmically along the radius attains a maximum $\sim\ln(R_0/d_0)$ in the corner region at the symmetry axis. On the other hand, according to Eq. (4) the characteristic magnitude of the concentration non-uniformity reduces with increase of stirring and, respectively, with reduction of $d_0$ as $\sim(1-k)v_0d_0/D$. Consequently, both these effects taken into account result in a reduction of the concentration maximum at the symmetry axis as $\sim d_0\ln(R_0/d_0)$ with increasing stirring and, respectively, reducing $d_0$.

## 7. Conclusions

We have studied in detail the concentration distribution resulting from a strong converging melt flow over a solidification front modeled by a disk of finite radius $R_0$. The velocity distribution was considered to be similar to that in the flow rotating over a disk at rest with the axial velocity component depending only on the axial coordinate and the radial velocity component depending linearly on the distance from the symmetry axis. This allowed us to obtain similarity and matched asymptotic expansion solutions showing that the radial solute concentration depends on the cylindrical radius $r$ as $\sim\ln^{1/3}(R_0/r)$ and $\sim\ln(R_0/r)$ close to the rim of the disk and at distances from it considerably larger than the solute boundary layer thickness, respectively.

The main conclusion is that flows converging along a solidification front, conversely to diverging ones, can cause a strong radial solute segregation with a logarithmic concentration peak at the symmetry axis. In converging flows, the solute concentration at the solidification front depends not only on the local velocity distribution, as it is the case in diverging flows, but also on the ratio of internal $d_0$ and external $R_0$ length scales which appears as a logarithmic correction factor to the result of a conventional order-of-magnitude estimate.

## Acknowledgement

Financial support from Deutsche Forschungsgemeinschaft in framework of the Collaborative Research Centre SFB 609 and from the European Commission under grant No. G1MA-CT-2002-04046 is gratefully acknowledged.

## Appendix A. Solution for the inner diffusion and intermediate layers

To solve Eq. (14) we introduce an intermediate axial coordinate $\zeta=\epsilon z$ and search for the solution as asymptotic series

$$F^{(\mathrm{i,m})}(z;\epsilon)\sim\sum_{j=0}\epsilon^j F_j^{(\mathrm{i,m})}(z) \tag{28}$$

for internal and intermediate regions denoted by indices i and m where $z\sim 1$ and $z\gg 1$, respectively. A bounded leading-order inner solution governed by

$$\frac{\mathrm{d}^2F_0^{\mathrm{i}}}{\mathrm{d}z^2}-z^2\frac{\mathrm{d}F_0^{\mathrm{i}}}{\mathrm{d}z}=0;\quad \left.\frac{\mathrm{d}F_0^{\mathrm{i}}}{\mathrm{d}z}\right|_{z=0}=0$$

is simply a constant $F_0^{\mathrm{i}}(z)=c_0^{\mathrm{i}}$. The corresponding intermediate solution governed by

$$\zeta\frac{\mathrm{d}F_0^{\mathrm{m}}}{\mathrm{d}\zeta}+\epsilon F_0^{\mathrm{m}}=0$$

is $F_0^{\mathrm{m}}(\zeta)=c_0^{\mathrm{m}}\zeta^{-\epsilon}$. For matching of both solutions an auxiliary intermediate coordinate $\tilde\zeta=\kappa z$ with $\epsilon\ll\kappa\ll 1$ is introduced that allows us to write

$$F_0^{\mathrm{m}}(\tilde\zeta)=\tilde c_0^{\mathrm{m}}\mathrm{e}^{-\epsilon\ln\tilde\zeta}\approx\tilde c_0^{\mathrm{m}}=c_0^{\mathrm{m}}\left(\frac{\epsilon}{\kappa}\right)^{\epsilon}$$

resulting in $\tilde c_0^{\mathrm{m}}=c_0^{\mathrm{i}}=c_0$. Then we obtain $F_0^{\mathrm{m}}(z)=c_0z^{-\epsilon}$ where $c_0$ is an unknown constant to be determined by the next-order inner solution governed by

$$\frac{\mathrm{d}^2F_1^{\mathrm{i}}}{\mathrm{d}z^2}-z^2\frac{\mathrm{d}F_1^{\mathrm{i}}}{\mathrm{d}z}=zc_0;\quad \left.\tau^\alpha\epsilon\frac{\mathrm{d}F_1^{\mathrm{i}}}{\mathrm{d}z}\right|_{z=0}=-1. \tag{29}$$

To eliminate $\epsilon$ from the boundary condition (29) we require $\tau^\alpha\epsilon=\alpha\tau^{\alpha-1}\sim 1$ that yields $\alpha=1$. Upon representing Eq. (29) in a selfadjoint form

$$\mathrm{e}^{z^3/3}\frac{\mathrm{d}}{\mathrm{d}z}\left(\mathrm{e}^{-z^3/3}\frac{\mathrm{d}F_1^{\mathrm{i}}}{\mathrm{d}z}\right)=c_0z,$$

we find

$$\frac{\mathrm{d}F_1^{\mathrm{i}}}{\mathrm{d}z} = -c_0 \mathrm{e}^{z^3/3} \int_z^\infty t\mathrm{e}^{-t^3/3}\,\mathrm{d}t = -c_0 3^{-1/3}\mathrm{e}^{z^3/3}\Gamma\left(\frac{2}{3},\frac{z^3}{3}\right), \tag{30}$$

where $\Gamma(a,x)$ is the incomplete gamma function [12]. The boundary condition in (29) leads to

$$c_0 = \frac{3^{1/3}}{\Gamma(2/3)} \approx 1.0651. \tag{31}$$

After some algebra one more integration of Eq. (30) yields

$$F_1^{\mathrm{i}}(z) = c_1^{\mathrm{i}} + \frac{c_0}{3}\frac{\partial}{\partial a} U\left(a,\frac{2}{3},\frac{z^3}{3}\right)\bigg|_{a=0}, \tag{32}$$

where $a$ is a formal parameter. The first-order intermediate solution is found similarly to the leading order one: $F_1^{\mathrm{m}}(\zeta) = c_1^{\mathrm{m}}\zeta^{-\epsilon}$. Now, taking into account that at the intermediate coordinate $z \gg 1$ and $\epsilon \ln z \ll 1$

$$F_1^{\mathrm{i}}(z) \sim c_1^{\mathrm{i}} - c_0 \ln\left(\frac{z}{3^{1/3}}\right) \tag{33}$$

and $F_1^{\mathrm{m}}(\tilde{z}) = \tilde{c}_1^{\mathrm{m}}\mathrm{e}^{-\epsilon\ln\tilde{z}} \sim \tilde{c}_1^{\mathrm{m}} = c_1^{\mathrm{m}}\left(\frac{\epsilon}{\delta}\right)^{\epsilon}$, while $F_0^{\mathrm{m}}(z) = c_0 z^{-\epsilon} \approx c_0(1-\epsilon\ln z)$ we obtain $\tilde{c}_1^{\mathrm{m}} = c_1^{\mathrm{i}} + c_0\ln 3^{1/3}$. To determine the constant $c_1^{\mathrm{i}}$ we have to consider the second-order inner solution. Note that $\epsilon$, in our case, is not a constant but a function of $\tau$ that is ignored by the ansatz (7). This fact taken into account results in an extra term in Eq. (14): $-z\frac{\mathrm{d}\epsilon}{\mathrm{d}\tau}\frac{\partial F}{\partial\epsilon}$ (see Eq. (17)). Further, taking into account $\frac{\mathrm{d}\epsilon}{\mathrm{d}\tau} = -\epsilon^2/\alpha$ and the asymptotic expansion (28) it is easy to see that Eq. (14) is accurate only up the first order in $\epsilon$. On the other hand, when both second order terms are taken into account, we find that they cancel mutually because of $\epsilon^2 + \frac{\mathrm{d}\epsilon}{\mathrm{d}\tau} = 0$ provided that $\alpha = 1$. Therefore, to obtain a non-zero next-order solution it is necessary to admit $\alpha = \sum_{j=0}\alpha_j\epsilon^j$ where $\alpha_0 = 1$. Then the next-order correction is $\sim\epsilon^3$ and the corresponding equation takes the form

$$\frac{\mathrm{d}^2F_3^{\mathrm{i}}}{\mathrm{d}z^2} - z^2\frac{\mathrm{d}F_3^{\mathrm{i}}}{\mathrm{d}z} = \alpha_1 z F_1^{\mathrm{i}}(z); \quad \frac{\mathrm{d}F_3^{\mathrm{i}}}{\mathrm{d}z}\bigg|_{z=0} = 0, \tag{34}$$

which can be solved similarly to the first-order one as

$$F_3^{\mathrm{i}}(z) = c_3^{\mathrm{i}} + \alpha_1\left(\frac{c_1}{3}\frac{\partial}{\partial a}U\left(a,\frac{2}{3},\frac{z^3}{3}\right)\bigg|_{a=0} + \frac{c_0}{9}\frac{\partial^2}{\partial a^2}U\left(a,\frac{2}{3},\frac{z^3}{3}\right)\bigg|_{a=0}\right).$$

The boundary condition in (34) yields $c_1^{\mathrm{i}} = c_0\psi(1)/3 = -c_0\gamma/3$, where $\psi(x)$ is the Psi (Digamma) function and $\gamma$ the Euler constant [12]. Eventually, we find

$$F_1^{\mathrm{i}}(0) = c_1^{\mathrm{i}} + \frac{c_0}{3}\frac{\partial}{\partial a}U\left(a,\frac{2}{3},0\right)\bigg|_{a=0} = c_0 c_1,$$

where

$$c_1 = \frac{1}{3}\left(\psi(1) - \psi\left(\frac{1}{3}\right)\right) = \ln\sqrt{3} + \frac{\pi}{6\sqrt{3}} \approx 0.8516. \tag{35}$$

## References


[1] D.T.J. Hurle, Handbook of Crystal Growth, vol. 2: Bulk Crystal Growth, Part B: Growth Mechanisms and Dynamics, Elsevier, 1994.

[2] J.A. Burton, R.C. Prim, W.P. Slichter, The distribution of solute in crystals grown from the melt. Part I: Theoretical, J. Chem. Phys. 21 (1953) 1987–1991.

[3] D. Camel, J.J. Favier, Theoretical analysis of solute transport regimes during crystal growth from the melt in an ideal Czochralski configuration, J. Physique 47 (1983) 1001–1014.

[4] D. Camel, J.J. Favier, Scaling analysis of convective solute transport and segregation in Bridgman crystal growth from the melt, J. Cryst. Growth 61 (1986) 125–137.

[5] J.P. Garandet, T. Duffar, J.J. Favier, On the scaling analysis of the solute boundary layer in idealized growth configurations, J. Cryst. Growth 106 (1990) 437–444.

[6] H. Schlichting, K. Gersten, Boundary Layer Theory, Springer, 2000.

[7] P.A. Davidson, Swirling flow in an axisymmetric cavity of arbitrary profile, driven by a rotating magnetic field, J. Fluid Mech. 245 (1982) 669–699.

[8] S. Yesilyurt, S. Motakef, R. Grugel, K. Mazuruk, The effect of the traveling magnetic field (TMF) on the buoyancy-induced convection in the vertical Bridgman growth of semiconductors, J. Cryst. Growth 263 (2004) 80–89.

[9] C.J. Chang, R.A. Brown, Radial segregation induced by natural convection and melt/solid interface shape in vertical Bridgman growth, J. Cryst. Growth 63 (1983) 343–364.

[10] J. Priede, G. Gerbeth, Breakdown of Burton–Prime–Slichter approach and radial solute segregation in converging flows, J. Cryst. Growth 285 (2005) 261–269.

[11] E.J. Hinch, Perturbation Methods, Cambridge University Press, 1991.

[12] A. Abramowitz, I.A. Stegun, Handbook of Mathematical Functions, Dover, 1972.

[13] C. Canuto, M.Y. Hussaini, A. Quarteroni, T.A. Zang, Spectral Methods in Fluid Dynamics, Springer, 1988.